Earth and Planetary Science Letters 516 (2019) 136–147

Contents lists available at ScienceDirect

Earth and Planetary Science Letters

www.elsevier.com/locate/epsl

Molards as an indicator of permafrost degradation and landslide processes

Costanza Morino [a,b,*], Susan J. Conway [b], Þorsteinn Sæmundsson [c], Jón Kristinn Helgason [d], John Hillier [e], Frances E.G. Butcher [f], Matthew R. Balme [f], Colm Jordan [g], Tom Argles [a]

[a] School of Environment, Earth & Ecosystem Sciences, The Open University, Walton Hall, Milton Keynes, MK7 6AA, UK
[b] Laboratoire de Planétologie et Géodynamique de Nantes UMR-CNRS 6112, 2 rue de la Houssinière, BP 92208, 44322 Nantes Cedex 3, France
[c] Department of Geography and Tourism, University of Iceland, Askja, Sturlugata 7, IS-101 Reykjavík, Iceland
[d] Icelandic Meteorological Office, Avalanche Centre, Suðurgata 12, Ísafjörður, Iceland
[e] Geography and Environment, Loughborough University, Loughborough, LE11 3TU, UK
[f] School of Physical Sciences, The Open University, Walton Hall, Milton Keynes, MK7 6AA, UK
[g] British Geological Survey, Environmental Science Centre, Keyworth, Nottingham NG12 5GG, UK

ARTICLE INFO

Article history:
Received 15 February 2018
Received in revised form 20 March 2019
Accepted 27 March 2019
Available online 17 April 2019
Editor: J.P. Avouac

Keywords:
molards
permafrost
landslide
Iceland
Mars

ABSTRACT

Molards have been defined in the past as conical mounds of debris that can form part of a landslide's deposits. We present the first conclusive evidence that molards in permafrost terrains are cones of loose debris that result from thawing of frozen blocks of ice-rich sediments mobilised by a landslide, and hence propose a rigorous definition of this landform in permafrost environments. We show that molards can be used as an indicator of permafrost degradation, and that their morphometry and spatial distribution give valuable insights into landslide dynamics in permafrost environments. We demonstrate that molards are readily recognisable not only in the field, but also in remote sensing data; surveys of historic aerial imagery allow the recognition of relict molards, which can be used as an indicator of current and past permafrost conditions. The triggering of landslides as a result of permafrost degradation will arguably occur more often as global atmospheric temperatures increase, so molards should be added to our armoury for tracking climate change, as well as helping us to understand landslide-related hazards. Finally, we have also identified candidate molards on Mars, so molards can inform about landscape evolution on Earth and other planetary bodies.

1. Introduction

Glacial and periglacial environments are particularly sensitive to the effects of climate change (Haeberli and Beniston, 1998; Hinzman et al., 2005). However, few easily recognisable landforms in cold landscapes are reliable indicators of increasing atmospheric temperature. Here, we propose that molards, landforms poorly reported in the literature, can help to fill this gap. Molards have been defined as conical mounds occurring in landslide deposits (Brideau et al., 2009; Cassie et al., 1988; Cruden, 1982; Geertsema et al., 2006b; Goguel and Pachoud, 1972; Jermyn and Geertsema, 2015; Lyle et al., 2004; McConnell and Brock, 1903; Milana, 2016; Mollard and Janes, 1984; Xu et al., 2012). They are generally ~0.3-12 m high (Brideau et al., 2009; Jermyn and Geertsema, 2015), up to 12 m wide (Milana, 2016), have a single, central, rounded to pointed summit (Jermyn and Geertsema, 2015; Xu et al., 2012), and flank slope angles of 27°-45° (Cassie et al., 1988; McConnell and Brock, 1903). Molards have been found in the distal zones, at the margins of the displaced mass, and/or below the main scarp of landslides (Cruden, 1982; Geertsema et al., 2006b).

Molards have recently been identified in a variety of periglacial environments, including northern Canada, the Andes, and the peaks of south-east Tibet (Jermyn and Geertsema, 2015; Milana, 2016; Xu et al., 2012). Three recent studies have hypothesised a link between molards and permafrost degradation (Brideau et al., 2009; Lyle et al., 2004; Milana, 2016). It is proposed that movement of landslide material in permafrost regimes causes blocks of frozen material to detach and be transported downslope (Brideau et al., 2009; Lyle et al., 2004). When the blocks come to rest, the ground ice cementing them thaws, leaving conical mounds of rocks and debris. Although no previous studies have observed the full cycle of molard evolution, original ground

* Corresponding author at: Laboratoire de Planétologie et Géodynamique, Université de Nantes, Bâtiment 4, 2 Chemin de la Houssinière, 44300 Nantes, France.
E-mail address: costanza.morino@gmail.com (C. Morino).

https://doi.org/10.1016/j.epsl.2019.03.040

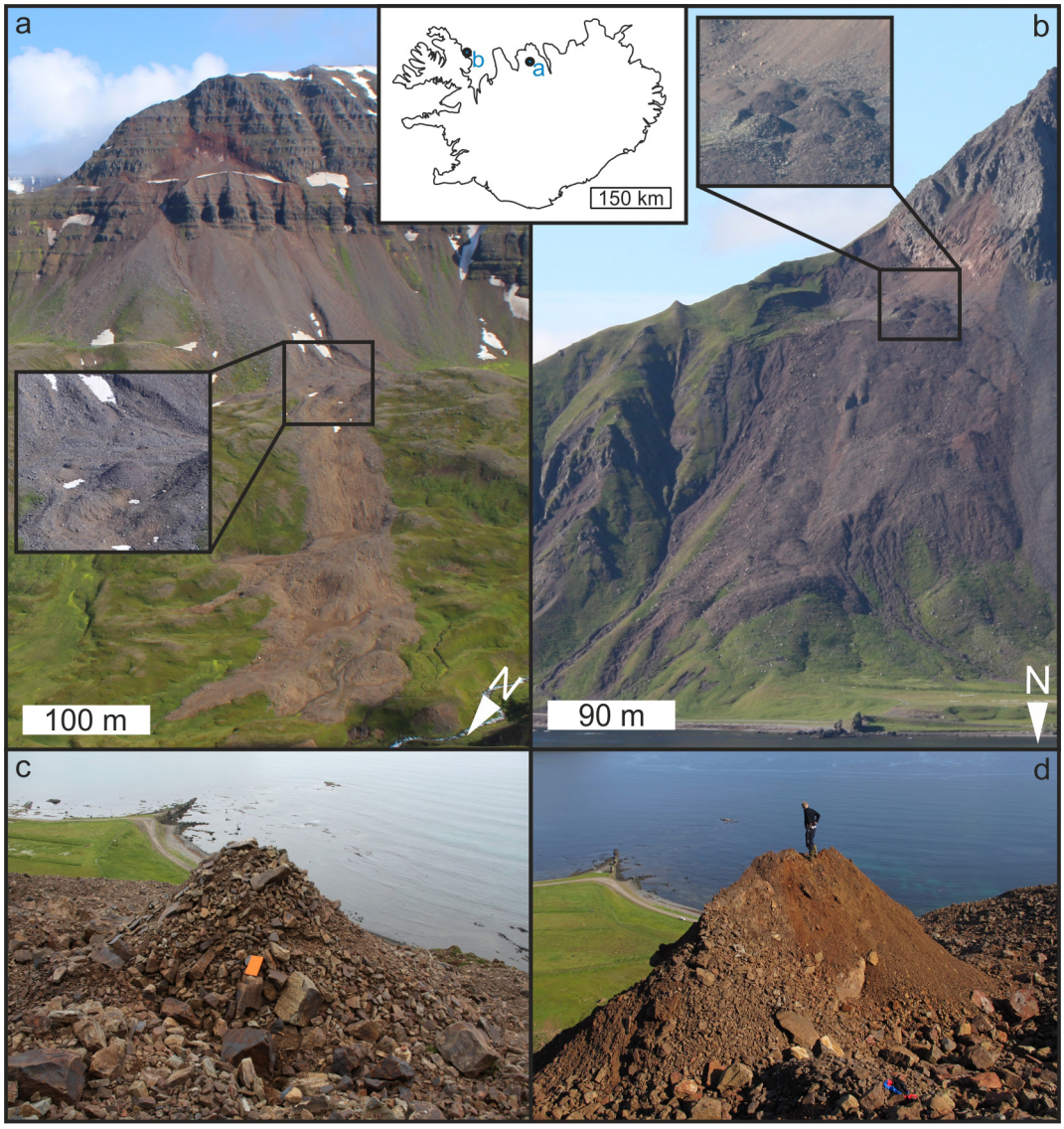

Fig. 1. The field sites. In the centre, an inset of the coastline of Iceland, with the location of the Móafellshyrna landslide as "a" and of the Árnesfjall landslide as "b". **a**, The Móafellshyrna landslide photographed in summer 2015, with an inset showing the molards. **b**, The Árnesfjall landslide photographed in summer 2016, with an inset showing the molards. **c**, A molard in Árnesfjall photographed 2 yrs after the landslide event and preserving the original preferential orientation of the source material (field notebook 19 × 13 cm as scale); note that the surface is clast-supported. **d**, A molard few days after the occurrence of Árnesfjall landside, preserving abundant fine deposits, person for scale.

ice contents of 50-80% have been estimated (Brideau et al., 2009; Milana, 2016) as sufficient for blocks of ice-cemented sediments to survive both initial failure and transport.

We studied molards found in two different landslides in Iceland: the first is located on the north-western side of Móafellshyrna Mountain (Tröllaskagi peninsula, Fig. 1a), and the second on the north-facing side of the Árnesfjall Mountain (Westfjords, Fig. 1b). The bedrock of both areas falls within the Tertiary Basalt Formation (Miocene-Lower Pliocene) (Jóhannesson, 2014), and is composed of basalts, rhyolites and weathered tephra layers. Both landslides originated from ice-cemented talus deposits perched on topographic benches. The Móafellshyrna landslide occurred on 20th September 2012 at 873 m a.s.l., travelled ∼1,300 m and mobilised ∼310,000 m^3 of material, while the Árnesfjall landslide occurred on 14th July 2014 at 418 m a.s.l., travelled ∼560 m and had a volume of ∼130,000 m^3. The preparatory factor for both landslides was intense precipitation, whilst permafrost degradation was the main triggering factor, with a minor role of seismic activity in the release of the Móafellshyrna landslide (Morino, 2018; Sæmundsson et al., 2018). Both landslides could be simply classified as debris slides (Varnes, 1978), but we show that molards allow the identification of additional failure dynamics.

We combine field and remote sensing studies of molards to constrain their complete evolution, providing the first observations before and after ice loss. These observations allow us to propose a definition of the term to adopt for molards in permafrost terrains: cones of loose debris that result from thawing of frozen blocks of ice-rich sediments mobilised by a landslide in permafrost terrains. Our data dispel any lingering doubts about the direct link between these landforms and permafrost degradation in cold environments. We show that molards in permafrost environments are a critical indicator of permafrost degradation, and they can reveal important information on the mobility of landslides in terrains affected by permafrost. We finally detail characteristics that can be used to identify them in the field and from remote sensing data.

2. Methods

2.1. Fieldwork

We conducted fieldwork of the Móafellshyrna landslide nine days after its occurrence and of the Árnesfjall landslide one day after the event. We revisited the Móafellshyrna site in summer 2015, three years after the landslide event, to perform field observations and ground-support for the collection of airphotos and airborne LiDAR (Light Detection And Ranging) data. We revisited the Árnesfjall site in summer 2016 to perform field observations and collect a Structure from Motion (SfM) photogrammetry dataset. We also performed differential GPS (dGPS) surveys of the landslides using two GNSS Leica System 1200 units in the Móafellshyrna site and two GNSS Leica VIVA GS10 System units in Árnesfjall site. One was used as a rover unit and the other one as base station, with the mean accuracy of measurements being 1 cm in the horizontal and 2 cm in the vertical direction. We investigated the interior of one molard at each site to determine their inner composition and structure.

2.2. Airborne data

In September 2015, the U.K. Natural Environment Research Council's Airborne Research Facility (NERC-ARF) on behalf of the European Facility for Airborne Research (EUFAR) collected aerial photography and LiDAR data for the Móafellshyrna area in Iceland, three years after the Móafellshyrna landslide occurred. 170 aerial photographs were collected with a Leica RCD105 digital camera, and 15 lines were flown to collect 126 million LiDAR points with 1.7 points/m^2 using a Leica ALS50-II. A GNSS Leica System 1200 dGPS was used in a fixed location at 1 Hz during the flight to collect base station data for the on-board dGPS. The geometric correction of the LiDAR point cloud was performed by NERC-ARF-DAN (Data Analysis Node) using the dGPS and navigational data. We used the LAStools extension for ArcGIS to convert the point clouds into gridded Digital Elevation Model (DEM) at 1 m/pixel, using the return time of the last peak of light to reach the receiver from the LiDAR laser shot (e.g., Höfle and Rutzinger, 2011; Jaboyedoff et al., 2012; Roering et al., 2013), which is usually assumed to be the ground return. We used Agisoft Photoscan Professional 1.3.5 to produce a seamless orthomosaic from the airphotos, where the position of the images was controlled using ten well-spread ground control points (GCPs) derived by locating matching positions between a hillshaded version of the LiDAR DEM and the airphotos. The combined uncertainty from the GCP placement and the processing with Agisoft is ∼1 m horizontally.

2.3. Structure from motion

For the Árnesfjall site, through the Structure from Motion (SfM) photogrammetry technique (Carrivick et al., 2016; Smith et al., 2015; Westoby et al., 2012) we produced a 3D topographic model, from which we also derived an orthomosaic at 9 cm/pixel and DEM at 18 cm/pixel. Photos were taken using a hand-held single-lens reflex (SLR) camera (Canon EOS 450D, 12.2-megapixel image sensor) from a ground-based oblique perspective at approximately 3 km from the landslide, using a fixed focal length of 200 mm with automatic exposure settings enabled. We identified clearly visible blocks and other features on the landslide — a total of 19 GCPs — and obtained their coordinates by using dGPS measurements. Prior to processing, photographs were inspected manually, blurry images were deleted, and the sky was masked out of each image manually. The remaining 73 photographs were imported into Agisoft Photoscan Professional 1.4.1. We removed any misaligned photographs after the initial alignment stage and then identified the GCPs in the image set, importing their coordinates recorded in the field by dGPS. The model was georeferenced using the 19 GCPs, for which we obtained a horizontal uncertainty of 0.05 m to 0.08 m, and a vertical uncertainty of 0.05 to 0.15 m. The 3D model has reconstruction errors of 0.9–1.8 pixels and an absolute precision of 0.5–1.5 m. We then imported the DEM and the orthomosaic into ArcGIS for further analysis.

2.4. Morphometric analysis of molards

In order to link the landslides' processes to the morphology of the molards, we i) analysed the molards' distribution and geomorphic characteristics, ii) compared the slope angle of their longer and shorter flanks, iii) calculated their eccentricity, and iv) plotted the orientation of their long axes with respect to those of the landslides.

2.4.1. Area, height, volume and slope characteristics

The molards were first digitised as a polygon in ArcGIS using their contrast in terms of texture and shading in the orthomosaics. The area of molards was estimated by calculating the area of the resulting polygon (Fig. 6e). To measure their height (Fig. 6e), for each molard we used a topographic profile placed parallel to the contour lines outside that molard and passing through its peak; the peak's elevation was read directly from the profile, with a representative elevation immediately outside the molard taken as its base. The elevation data for these profiles were derived from LiDAR in the case of Móafellshyrna and SfM in the case of Árnesfjall. The volume of material composing the molards was calculated following Conway and Balme (2014), reconstructing the surface of the landslide without the molards, and deriving the deposited volumes by subtracting this surface from the surface with the molards (Fig. 6e). Error propagation calculations by Conway and Balme (2014) suggest that such volume estimates are accurate to within 15%. Slope of the basal area where molards lie was calculated by creating a slope map of the surface of the landslide without the molards and taking the mean value. The slope angle for the long and short flanks of molards was the mean value of the slope obtained from the slope map of the original DEMs (Fig. 6e).

We performed two-sample t-tests assuming unequal variances for the volume, area, height, slope angle of the basal area and eccentricity of molards, using the values of Móafellshyrna and Árnesfjall respectively as variables. We used the values of each site separately for testing the slope angles of short and long flanks of their molards (see Supplementary Table 1).

A dispersion parameter $\psi = \sigma/\mu$ (where σ is the standard deviation and μ is the mean) for height, axes and volumes of molards, show less homogeneous sizes in Móafellshyrna compared to those of Árnesfjall (see Supplementary Table 2). This is confirmed by Pearson correlation coefficient calculated for height-long axis, height-short axis and long-short axis, showing a strong correlation in Móafellshyrna, suggesting a circular shape in plan-view and casually linked dimensions, while in Árnesfjall lower values suggest more elliptical shapes (see Supplementary Table 2).

The volume-frequency distribution for the molards in Móafellshyrna shows a power-law distribution, while the volume-frequency distribution for the molards in Árnesfjall conforms to an exponential distribution (see Supplementary Fig. S1). Both were determined by comparing three different plots of the volume-frequency distribution (i.e., linear-linear, logarithmic-linear, bi-logarithmic), where we considered the best distribution the one fitting the more to a straight line.

2.4.2. Eccentricity and direction

To measure the eccentricity of the molards, an ellipse was fitted to approximate the perimeter of each molard, with the area of

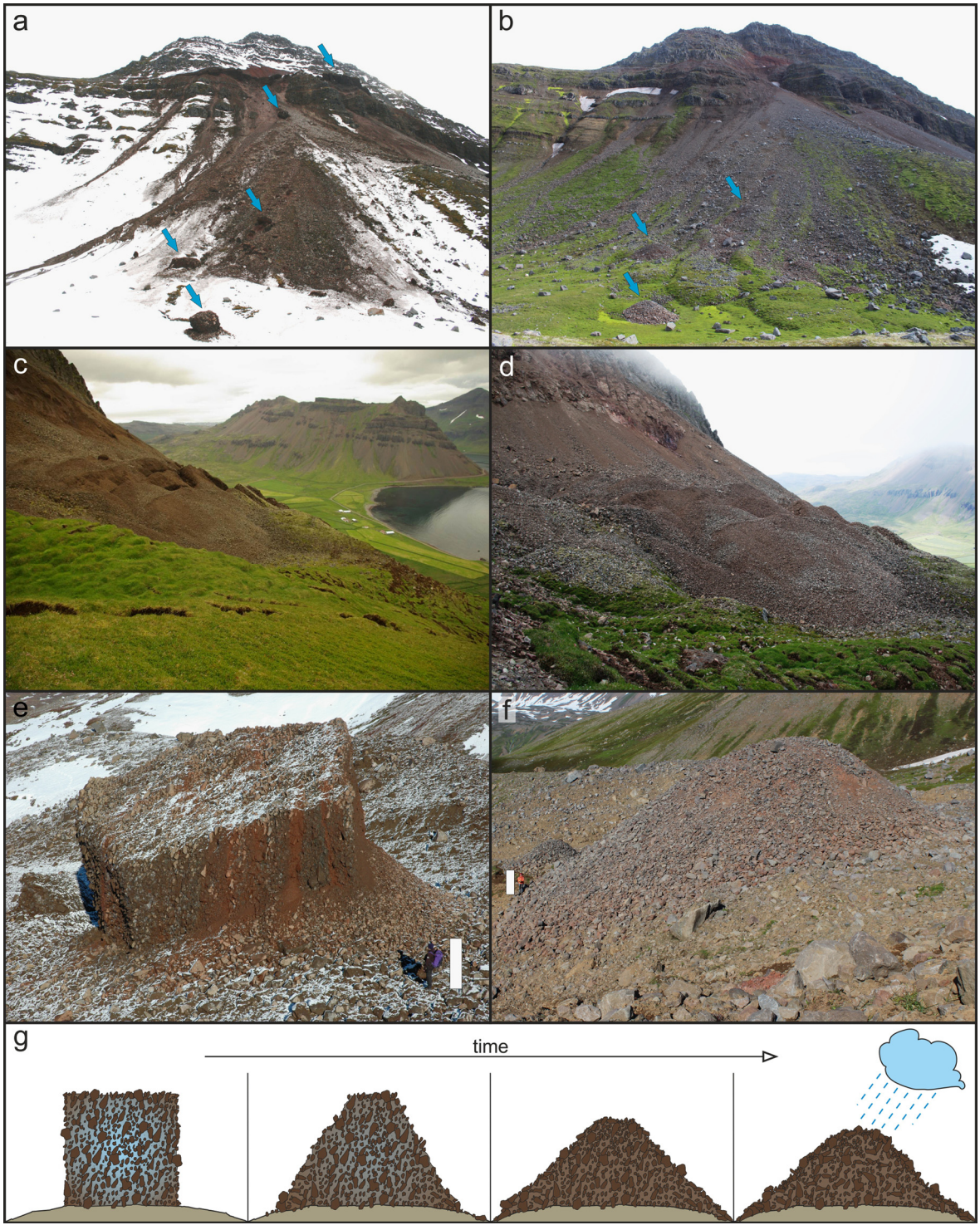

Fig. 2. The formation of molards. In each pair of images, ice-cemented blocks are on the left; the resulting molards are on the right. **a**, Cubic and angular blocks of ice-rich sediments (blue arrows) at the Móafellshyrna site that are perched on the source area and have fallen onto the talus slope below (the block in the foreground is ~7 m wide). Photo taken the day after the failure (courtesy of G. Hansson). **b**, Similar perspective as in **panel a**, but three years after the failure, with remnants of the blocks of ice-rich sediments preserved as molards (blue arrows; the molard in the foreground is ~9 m wide). **c**, Angular ridges generated by tilting of ice-cemented talus at the Árnesfjall site (up to ~4 m high). Photo taken two days after the failure (courtesy of V. Benediktsson). **d**, Similar perspective as **panel c**, but two years after the failure, where remnants of the ice-cemented ridges have degraded into densely-packed, elongated mounds of debris (up to 3.7 m high). **e**, The largest block of ice-rich sediments that fell during the Móafellshyrna event; note different layers of deposits composed of imbricated boulders, cobbles, and pebbles embedded in brown to red sandy to silty clay (the white bar next to the person as a scale indicates 2 m height). **f**, The remnant of the block in **panel e** three years after the failure, preserved as a molard (the white bar next to the person as a scale indicates 2 m height). **g**, Side-view schematic evolution of a molard, from the block of clast-supported imbricated talus deposits cemented by ground-ice (bluish colour) to the collapsed conical mound of debris, preserving sorted gravel deposits on its surface (dark brown), with fine deposits (light brown) being leached out. (For interpretation of the colours in the figure(s), the reader is referred to the web version of this article.)

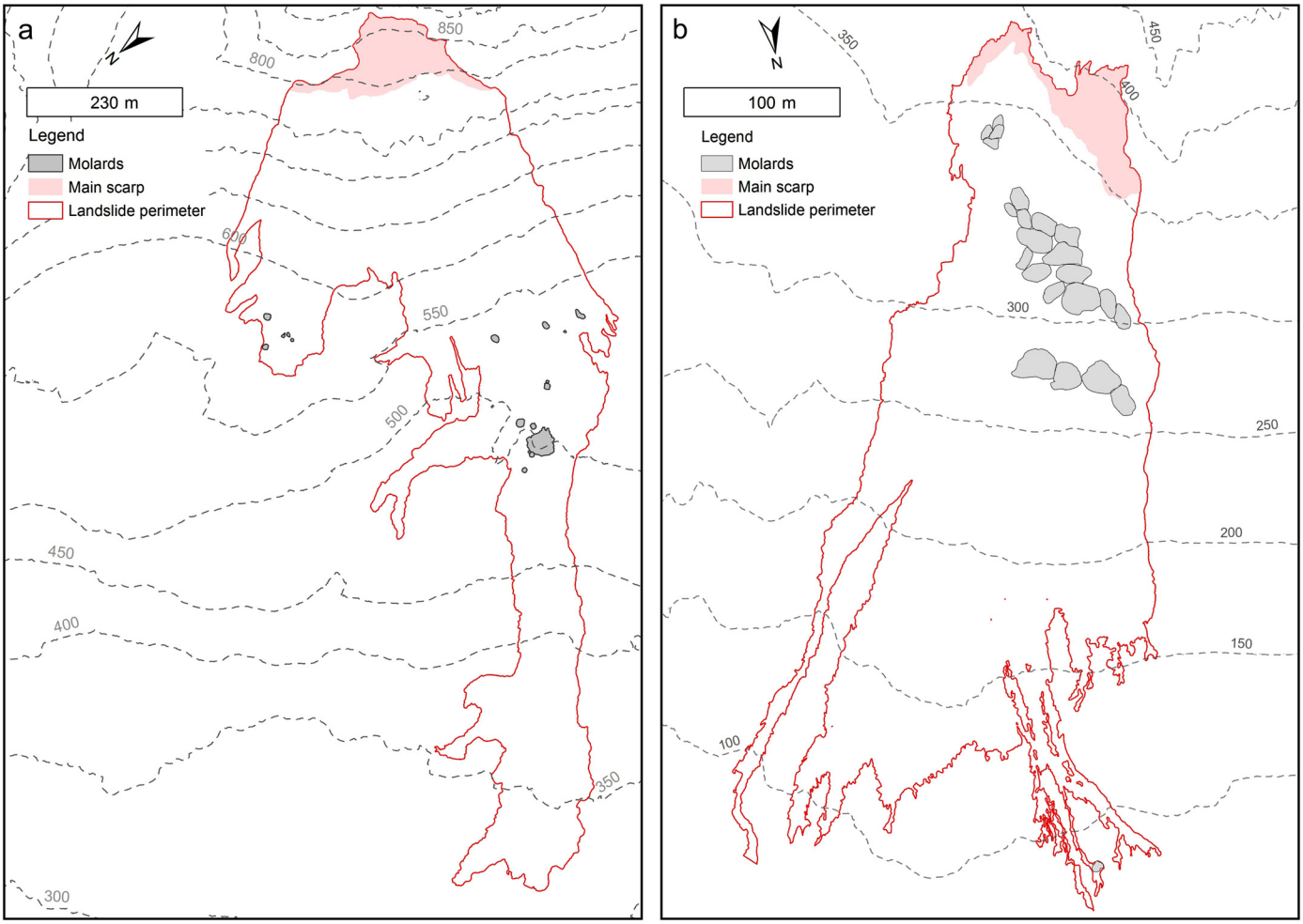

Fig. 3. Maps of the landslides. a. A contour map with a line map of the Móafellshyrna landslide, with its main features and perimeter and location of the molards indicated. **b.** A contour map with a line map of the Árnesfjall landslide, with its main features and perimeter and location of the molards indicated.

each ellipse being equal to the area of the perimeter of the represented molard. Then, the eigenvalue and eigenvectors of each zone were calculated, with the orientation of the ellipse being in the direction of the first eigenvector (Jorge and Brennand, 2017). Finally, the geometric characteristics of the ellipse were calculated, specifically the centroids, the major and the minor axes (the ratio of the major and minor axes of the ellipse is the same as the ratio of their eigenvalues). We plotted the orientation of the long axes of the molards against the propagation direction of the landslides using GeoRose open-source software (Fig. 6b, d).

3. Results

3.1. Molard formation in permafrost terrains

During the field observations performed immediately after the failures, in the Móafellshyrna landslide deposits we found isolated pseudo-cubic and angular blocks of ice-rich sediments (Fig. 2a, e) that came to rest at the foot of the talus slope where the topography flattens (Fig. 2a), 295-390 m below the source area (Fig. 3a). At Árnesfjall, we found a spatially dense group of angular, elongated ice-cemented ridges of debris 40-150 m below the top of the main scarp of the landslide (Figs. 2c, 3b), and an isolated block of ice-rich sediments at the toe of the landslide. In both landslides, the blocks and ridges were composed of poorly-sorted clast-supported talus deposits. Ground-ice was cementing the material, allowing the blocks and ridges to preserve a cubic or angular shape (Fig. 2a, c) both during and immediately after the failure. We examined the lithological and grain-size composition of the blocks and ridges of ice-rich sediments. They comprised slightly imbricated angular boulders, cobbles, and pebbles embedded in a variably abundant sandy silt to silty clay matrix. The colour of the matrix varied from brown to red, and the lithology of the clasts reflects the bedrock of the area (Tertiary Basalt Formation), with abundant fines originating from the weathered volcanic lithologies.

We revisited the Móafellshyrna and Árnesfjall sites 2 and 3 yrs after the failures, respectively. In Móafellshyrna, we found conical molards with rounded summits in the place of the original ice-cemented blocks (Fig. 2b, f). In Árnesfjall, the elongate ridges in a group below the main scarp had become smaller (with maximum height of 3.7 m) molards with the same elongated shape and pointed summits (Fig. 2d). Therefore, at both sites the molards are secondary features generated by the thaw of the ice cementing the frozen blocks or ridges, which were produced as primary features by the two landslides. At both sites, at the surface most molards are clast-supported (by boulders, cobbles and pebbles; Figs. 1c, 4a), with fine material sometimes present, but there are rare cases of molards composed of matrix-supported gravelly sand to silty clay material (Fig. 1d). However, the surface material does not necessarily reflect the inner composition of molards; in the interior, the deposits are richer in matrix just a few decimetres below the surface (Fig. 4b). Once the blocks disaggregated into molards, we observed that some of them still preserved a faint hint of the original layering of the source deposits (Fig. 1c), with imbricated

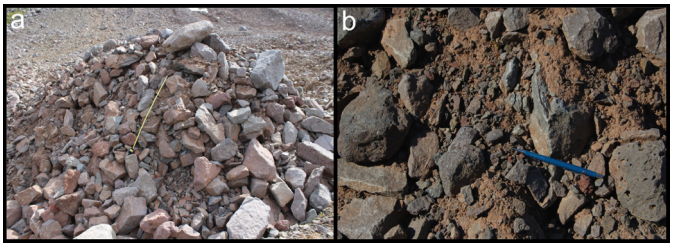

Fig. 4. Material comprising molards. a, A molard in Móafellshyrna showing coarse deposits on the surface with no gradation or preferential orientation (measuring tape extended to 1 m as scale). **b**, Internal composition of a molard, comprising unsorted gravel in sandy silt to silty clay matrix (the pen is 10 cm long).

unsorted gravel in sandy silt to silty clay matrix, which is further proof that the deposits must have been ice-cemented during the failure. However, in most of the cases, molards comprised non-stratified unsorted gravel to clay material, and we did not observe any radial grain size gradation (Fig. 4a, b).

A schematic evolution of the degradation of ice-cemented debris material into a molard has been recently proposed (Milana, 2016), where the author assumed a sphere as the theoretical initial shape of the frozen mass. We found that molards with different shapes are a direct result of the different shapes of the original blocks of ice-cemented material. From a cubic or angular block, the resulting molard has a rounded and symmetrical conical shape (Fig. 2e-g); alternatively, in the case of ice-cemented elongated ridges, the final molards preserve the elongated shape. In both cases, we found that molards can have up to 30% lower relief than the initial block, because thaw results in the debris located at the top of the block/ridge collapsing to its base (Fig. 2g). Assuming that ice only fills the pore-space, we can estimate the original size of a block of ice-rich sediments from the resulting molard. Knowing the height (h) and length of the flank (L) of a molard, it is possible to estimate the width (B) – and then the area and volume – of the original block as shown in equation (1) (Fig. 5):

$$B = 2\sqrt{L^2 - h^2} \tag{1}$$

We have tested this model through field measurements of the size of the largest block of ice-rich sediment. A molard of $L = 11.9$ m and $h = 10.2$ m will result from a block with $B = 12.2$ m, which is approximately the measured length of the biggest block in Móafellshyrna after the failure. So for example, from a cubic and angular block 10.2 to 14.8 m high and with an area from 924.24 to 1002 m^2, the resulting molard would have a rounded and symmetrical conical shape, would stand 10.2 m high maximum and cover an area of 1193 m^2. If molards obey this relation, then this model gives an estimation of the maximum initial ground ice content of the original blocks.

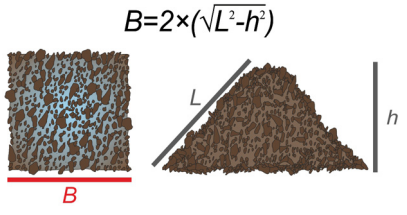

Fig. 5. From block to molard. Model for estimating the width of the original block of ice-rich sediment (assumed to have a rectangular section) knowing height and length of the flank of the molard, which is assumed to have a triangular section.

A similar surface lowering (35%) has been recorded in hummocks of thawing ice-cored moraines in the terminal region of outlet-glaciers in Iceland (Krüger and Kjær, 2000). Hummocks of ice-cored moraines are similar to molards not only in their conical shape, but also in their mode of formation: ice-cored moraines retain massive ice cores and form hummocks when the ice melts (Dyke and Savelle, 2000). Similarly to molards, the form of the hummocks is determined by thaw and gravitational collapse. They can have similar flank slope angles to molards of between 25° and 35° (Hambrey et al., 1997) or higher. Many meters of ice can be buried under only a few centimetres to meters of till (Schomacker and Kjær, 2008), meaning that ice-cored hummock can easily disappear completely when all the ice is melted (Mercer, 1963). The ratio of ice to debris within molards in Móafellshyrna is much lower (15-20% ground ice content estimated from visual inspection; Sæmundsson et al., 2018), giving them a much higher preservation potential than hummocks in ice-cored moraines. This is why molards remain recognisable even after the ice has gone.

We posit that molards should vary in shape and size depending on i) the slope on which they form, ii) their ice content and granulometry, and iii) the emplacement dynamics of the host landslide. Circular molards with rounded summits are found on relatively low slopes (<17° in Móafellshyrna), whereas those with angular summits and elongate shapes are found on relatively high slopes (28° in Árnesfjall). Based on arguments of angle of repose for loose granular materials (Carrigy, 1970; Pohlman et al., 2006; Van Burkalow, 1945), molard shape should vary with granulometry, but we have no specific observations to substantiate these relationships. Our observations show that molards in permafrost terrains derive from the thaw of the ground ice cementing loose deposits, therefore molards cannot form without ground ice. This cements the loose material, allowing it to behave like a solid during transport, and once thawed induces collapse of the material into molards. Our observations suggest that the higher the initial ground ice content the lower the final height of the molard, compared to the initial frozen block, hence, the lower its flank slopes and the more domed its summit. If the amount of ground ice is far in excess of the pore space, we expect them to behave like hummocks in ice-cored moraines. We infer that the lack of matrix observed at the surface of the molards years after their deposition and degradation is due to the action of precipitation, washing out the fines through the coarse debris by percolation (Fig. 2g). Finally, the shape and size of the molards also depends on the mechanism of emplacement of the landslide, and we report on this in the following section.

3.2. Molard distribution and morphology: indicators of landslide dynamics

The morphometry and the spatial distribution of molards in Móafellshyrna and Árnesfjall landslides provide information about the failure dynamics of the landslides. Molards act like tracers, because during transport they behave like solid blocks and thus we know where they originate. Molards in Móafellshyrna have different characteristics to those in Árnesfjall, although the average height, basal area and volume of the molards do not differ significantly between the two landslides (Supplementary Table 1). For instance, the Móafellshyrna molards have a larger range in volumes (Fig. 6e). Also, the slope angles of the short and long flanks of molards are roughly equal in Móafellshyrna (Fig. 6e), while the downslope faces of the Árnesfjall molards are longer and less steep than the scarp-facing short flanks (Supplementary Table 2, Fig. 6e). The Árnesfjall molards are consistently elliptical in shape (Figs. 3b, 6e), whereas molards in Móafellshyrna are variable, but generally closer to circular (Figs. 3a, 6e). Finally, while Móafellshyrna molards do not show a preferential orientation in their long axes with respect to the landslide's runout-direction (Fig. 6b), the long axes of the molards in Árnesfjall are oriented roughly perpendicular to the landslide's runout direction, and parallel to the main scarp (Fig. 6d).

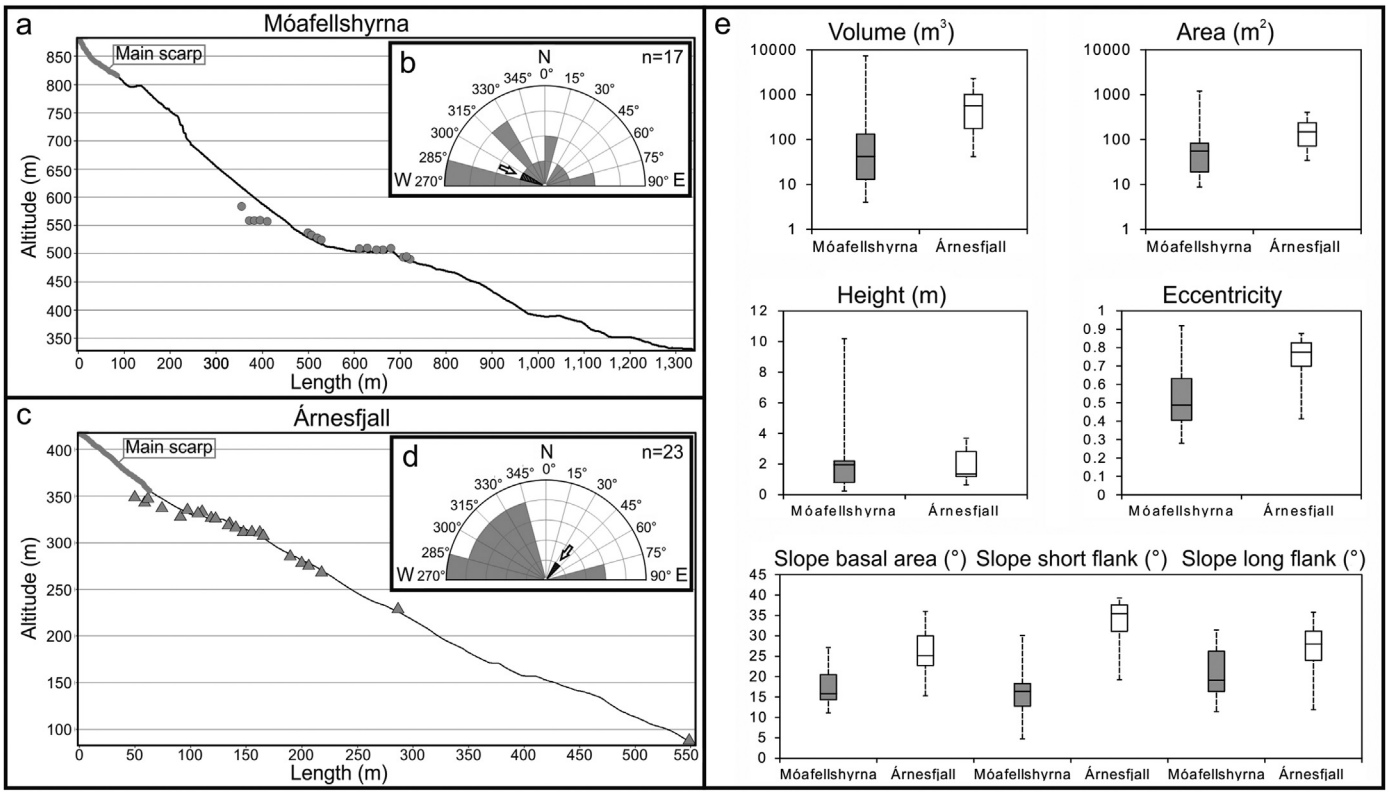

Fig. 6. Dimensions and distribution of molards. a, The topographic profile of the Móafellshyrna landslide, with the position of molards marked as grey points, and the main scarp zone marked with a thick grey line. **b**, Rose diagram of the orientation of molards' long axes where the orientation of the Móafellshyrna landslide is marked as a hatched texture and by an arrow. **c**, The topographic profile of the Árnesfjall landslide, with the position of molards marked as grey triangles, and the main scarp zone marked with a thick grey line. **d**, Rose diagram of the orientation of molards' long axes where the orientation of the Árnesfjall landslide is marked as a hatched texture and by an arrow. **e**, Boxplots of the volume, area, height, slope of the basal area, slope of the short and long flanks, and eccentricity of the molards in Móafellshyrna and Árnesfjall; note that the vertical axis for volume and area use a logarithmic scale. The whiskers indicate the maximum and minimum values, the boxes mark the interquartile range, and the black lines are the medians of each population. For all the measurements, in Móafellshyrna $n = 17$, in Árnesfjall $n = 23$.

In Móafellshyrna, the molards are clustered in an area with a mean slope of 17° at the foot of, or beyond, the talus slope located below the topographic bench (Fig. 6a). Their position matches that expected for rockfalls, where competent fragments detach and fall, and come to rest either within, at the foot, or beyond the base of the talus slope (Evans and Hungr, 1993; Varnes, 1978). The large size variation of molards in Móafellshyrna mirrors that in rockfall processes (Fig. 6e), where their power-law frequency–volume distribution (Supplementary Fig. S1) is related to rock fragmentation (e.g., Dussage-Peisser et al., 2002; Dussauge et al., 2003; Einstein, 1937). Their final position on a low slope allowed the ice-cemented blocks to degrade into isolated molards with a circular base, radially symmetrical flank slopes (see Fig. 6e, Supplementary Table 2), and no preferential orientation.

Molards in Árnesfjall lie on an average slope of 26° and are concentrated less than 30 m below the base of the failure scarp (Fig. 6c). This position is typical of the location of *en echelon* concave-upward rupture surfaces in debris slides (Hungr et al., 2001). These ruptures are oriented perpendicular to the flow direction, and blocks of material often move downward with little internal deformation (Varnes, 1978). Molards in Árnesfjall derive from the degradation of densely-grouped, elongated ice-cemented ridges exposed by the rotational-sliding motion of the source material, cut by several curved planes of movement. These dynamics are reflected in their more homogeneous size (see Supplementary Table 1) and their elliptical shape (Fig. 6e), a result of the degradation of elongated cusps of ice-cemented precursor units produced by relatively coherent rotational sliding. This process can be deduced by the orientation of the molards' long axes, perpendicular to the main movement downslope (Fig. 6d). The steep upslope-facing short flanks of these molards (Figs. 2c, d, 6e) reflects a common behaviour of rotational slides, where the upper part of the units produced by curved rupture surfaces tilt backwards toward the scarp.

By measuring the size, morphology and distribution of molards, we have been able to discriminate between the processes of simple gravitational fall in the Móafellshyrna case and of rotational sliding in the Árnesfjall case. We recognise that other types of motion might also transport ice-cemented materials, forming molards, once the ice has thawed, with morphometry and distribution different to those described here. For example, molards with a wide-range of dimensions scattered across the mobilised mass could be expected in rock/debris avalanche deposits, due to the entrainment of the ice-cemented blocks in their extremely rapid flow-like motion (Hungr et al., 2001). Molards accumulated in the terminal lobe of debris-flow deposits could result from the degradation of blocks of ice-rich sediments transported by the flow, due to their tendency of producing longitudinal sorting near the front of the surge (Iverson, 1997).

3.3. Molards in remote sensing data

Identifying molards reliably is crucial if they are to give insights into the geomorphological and climatic condition of the landscape where they form.

In addition to molards being readily identifiable in the field, we propose that in most cases they can also be reliably identified in remote sensing data, although field studies would be needed to confirm their identification as molards. In Fig. 7, we show a plan view image of molards in Móafellshyrna landslide (Fig. 7a, b), a lo-

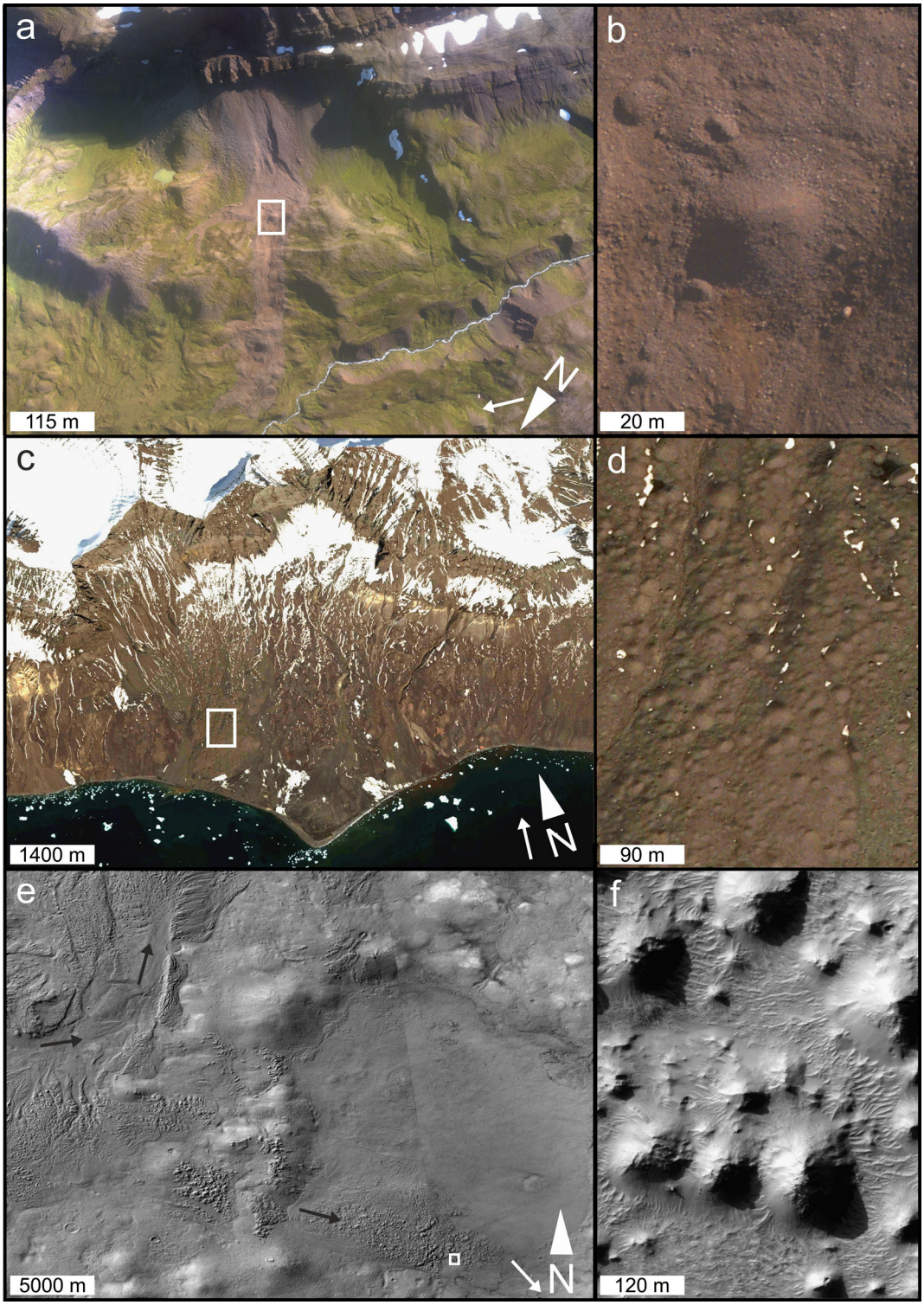

Fig. 7. Molards from remote sensing. a, Aerial image of Móafellshyrna landslide, with the white box outlining the extent of **panel b**. **b**, Molards in Móafellshyrna landslide. White arrow in **panel a** indicates the lighting direction in **panels a** and **b**. **c**, Aerial image of a rock avalanche on the south coast of Nuussuaq, west coast of Greenland (image from Google Earth) with the white box outlining the extent of **panel d**. **d**, Candidate molards in Nuussuaq (image from Google Earth). White arrow in **panel c** indicates the lighting direction in **panels c** and **d**. **e**, Impact ejecta flow deposits from Hale Crater on Mars, (Context Camera images G14_023858_1429 and G19_025704_1431, credit NASA/JPL-Caltech/MSSS), with black arrows indicating the inferred flow directions and white box indicating the position of **panel f**. **f**, Conical landforms in the ejecta blanket of Hale Crater on Mars (High-resolution Imaging Science Experiment image ESP_052222_1425, credit NASA/JPL/University of Arizona). White arrow in **panel e** indicates the lighting direction in **panels e** and **f**.

cation with candidate molards elsewhere on Earth (Fig. 7c, d), and possible candidates on Mars (Fig. 7e, f). In Fig. 7d, cone-shaped landforms of ~1-46 meters-diameter are scattered across the surface of deposits mobilised by a rock avalanche (Pedersen et al., 2002) in Greenland. The failure falls within a region where landslides have been active for the last 10,000 yrs (Dahl-Jensen et al., 2004) and continuous permafrost has been reported (Van Tatenhove and Olesen, 1994). Hence, we infer that these conical mounds

are molards, and *in situ* investigations have confirmed this hypothesis (Benjamin et al., 2018; Pedersen et al., 2001; Stuart Dunning, *pers. comm.*) providing strong evidence of the occurrence of permafrost degradation in this area. Many more candidate molards are seen here than in our Icelandic examples, suggesting that more molards could be produced in areas with more pervasive ground ice.

Similar scattered conical landforms are identifiable within impact ejecta originating from Hale Crater on Mars (Fig. 7e, f). The ice-rich nature of the impact ejecta has already been proposed based on other landforms (e.g., Jones et al., 2011). We propose that conical landforms within the ejecta flow are molards, which with further study could yield important constraints on the ice-content of the original ejecta flow and insights into recent modification of ground ice reservoirs on Mars.

4. Discussion

Iceland has discontinuous permafrost (Rekacewicz, 2005), which in general is spatially and temporally heterogeneous (Rödder and Kneisel, 2012), and mountain permafrost has been modelled at elevations above 800-900 m a.s.l. in the central-northern regions of the island (Etzelmüller et al., 2007). This predicted permafrost distribution has been ground-truthed by comparison with the distribution of active rock glaciers and ice–cored moraines in the Tröllaskagi peninsula (Farbrot et al., 2007; Lilleøren et al., 2013). The Móafellshyrna landslide falls within the predicted spatial zone and altitude band for mountain permafrost. In contrast, the Árnesfjall landslide occurred on the coastline of the Westfjords, 400 m below the predicted permafrost altitude. However, at the Árnesfjall site the elevation for permafrost could be significantly lower than the one predicted by Etzelmüller et al. (2007) and Farbrot et al. (2007), because of lower summer temperatures, shorter melting season and the proximity at less than 25 km of the Drangajökull ice cap, around which the presence of permafrost has been hypothesised, but never confirmed (Brynjólfsson et al., 2014; Hjort et al., 1985). Hence, the presence of molards here is the only unequivocal and pragmatically detectable indicator of permafrost conditions. Both landslides originated from talus material. In general, coarse blocky talus material is a particularly favourable substrate for ice-rich permafrost (Etzelmüller et al., 2001; Harris and Pedersen, 1998). In talus slopes, ground ice can be formed by burial of snow by mass wasting debris, which protects the snow from ablation (Gruber and Hoelzle, 2008), and can lead to the development of ice-rich permafrost (Kenner et al., 2017). Annual freeze-thaw cycles in talus slopes in mountain permafrost environments can reach depths of ∼3-7 m, but rarely decametres (Matsuoka et al., 1998). The ice-cemented blocks that detached in the Móafellshyrna landslide were 15-20 m thick, much larger than the expected maximum depths of annually-formed, ice-cemented ground. Hence, the source talus slopes were perennially-frozen ground and the molards here indicate permafrost degradation. Furthermore, permafrost degradation due to anomalous rise in temperature has been recognised as the main trigger for the Móafellshyrna landslide (Sæmundsson et al., 2018).

In the few works where they have been reported, molards are generally defined as conical mounds occurring in landslide deposits (Cassie et al., 1988; Goguel and Pachoud, 1972; Mollard and Janes, 1984). However, the application of the term “molard” has not been consistent. For example, Cassie et al. (1988) described “molards” in the Frank Slide, following the terminology of Mollard and Janes (1984): “one of a series of conical mounds of broken slide rock deposited along the typically lobate margin of rock avalanche spoil debris; a debris cone”. However, in later literature (e.g., Charrière et al., 2016), the same mounds at Frank Slide are called “hummocks”. Recently, Brideau et al. (2009) and Milana (2016) moved from a morphological to a process-related definition of molards, as they hypothesised that landslides in permafrost terrains could mobilise blocks of frozen material, which degraded into cones of debris – molards – once at rest. Since in the past the terms “molards” and “hummocks” have been used interchangeably, which can lead to confusion, and since the majority of the cases of molards in the literature are reported to have formed in permafrost/cold terrains (Brideau et al., 2009; Jermyn and Geertsema, 2015; Lyle et al., 2004; Milana, 2016; Schwab et al., 2003; Xu et al., 2012), a refinement of the definition of molards occurring in permafrost environments is necessary. Here, we develop on the recent definition of molards of Brideau et al. (2009) and Milana (2016) by providing the missing field evidence to demonstrate the entire formation-history of molards in permafrost environments that allow us to refine their definition: cones of loose debris that derive from the thaw of blocks of ice-rich sediments mobilised by landslides in permafrost terrains. They are secondary features, resulting from the primary emplacement of initially frozen ice-cemented blocks/ridges within landslides, which degrade into conical mounds as the ice thaws in their new position. Molards reported in landslides have often involved terrains that are known to be affected by discontinuous permafrost (Brideau et al., 2009; Lyle et al., 2004). In one case, the deposits of an active rock glacier were the source material for the landslide with molards (Milana, 2016). As we have shown that molards in cold environments evolve from parent blocks of ice-rich sediments, insights from this study allow previously reported molards in permafrost environments to provide new information: they can be an indicator (perhaps the only indicator) of ongoing or past permafrost degradation in permafrost terrains. In Móafellshyrna, molards are the first direct indication of ongoing permafrost degradation in this region of Iceland, in an area already thought to host mountain permafrost (Etzelmüller et al., 2007; Farbrot et al., 2007; Lilleøren et al., 2013). In Árnesfjall, molards mark both the presence of permafrost in an area thought to have no perennially frozen ground and its recent/ongoing degradation.

Our new recognition that molards provide a way to track permafrost degradation is important, as similar indicator-landforms (such as retrogressive-thaw slumps (Ashastina et al., 2017), thermokarst lakes (Yoshikawa and Hinzman, 2003), baydjarakhs (Séjourné et al., 2015) are scarce, and generally occur only in zones of continuous permafrost. Other indicators of permafrost, such as active rock glaciers, ice-cored moraines, composite ridges, ice-wedges, or palsas, need long-term monitoring of air/ground temperature to detect the state of permafrost, whereas molards directly reveal permafrost degradation. We propose that future studies can use molards with the purpose of mapping historic-permafrost conditions and geographically tracking past climate change.

Molards could perhaps be confused with hummocky terrains found in debris/rock-avalanche deposits. Hummocks are mounds, blocks and ridges that characterize large landslides and debris/rock avalanches (Paguican et al., 2014; Shea and van Wyk de Vries, 2008; Siebert, 1984; Ui, 1983; Yoshida et al., 2012). Hummocks result from the formation of horsts and grabens during transport and spreading or by stretching around blocks by faults (Davies et al., 2013; Glicken, 1996; Glicken et al., 1981; Shea et al., 2008; Voight et al., 1981), and their shapes can be used to determine the kinematics of a landslide (Shea and van Wyk de Vries, 2008). Hummocks in debris/rock-avalanche deposits are characterised by pervasive shattering or jigsaw fracturing as result of brittle deformation associated with the transport of large rock masses (e.g., Calvari et al., 1998; Shreve, 1968; Ui et al., 1986; Yarnold and Lombard, 1989). Hence, hummocks should differ sedimentologically from molards in permafrost terrains, but this would require further data collection to fully substantiate. Many processes can

generate conical mounds, but molards in permafrost terrains are always associated with a landslide. Molards in permafrost terrains would not form without ground ice; this makes the debris material behave like solid blocks during the failure and transport because of its cementing action, and allows the formation of discrete mounds of loose debris (molards) via melting. No ice is involved or is necessary in the formation of hummocks, while it is instead the primary factor in the formation of molards in permafrost environments. When studying molards, it is important to consider the geomorphological and environmental setting where they are found. There are examples in the literature of other mounds and ridges that have similar characteristics to the molards reported here. Some have been observed in mountainous non-permafrost terrains, others at the limits of discontinuous permafrost, or in paraglacial environments, but have not been linked to permafrost degradation (Blais-Stevens et al., 2015; Dufresne et al., 2018; Geertsema et al., 2006a; Schwab et al., 2003). These include for example ridges and hummocky topography that are considered evidence of spreading during the motion of the Mink Creek landslide, north-western British Columbia, involving glaciomarine sediments in a non-permafrost area (Geertsema et al., 2006a), and similar ridges were observed in other spreading processes in Québec (Carson, 1979). Conical features and ridges up to 5 m high are thought to have been produced by the fragmentation of basalt-boulders transported by the Sutherland landslide, British Columbia, in an area not affected by permafrost (Blais-Stevens et al., 2015). In 2015, a landslide occurred at the terminus of Tyndall Glacier in Alaska, traversed the width of the Taan fjord, and re-emerged onto land depositing mounds and hummocks that preserved the source stratigraphy, but no ice was observed within the deposits (Dufresne et al., 2018). Molards have been reported in a recent rock avalanche in west central British Columbia, where the role of degrading mountain permafrost in the release of the failure is inferred, but the permafrost parameters were not studied (Schwab et al., 2003). In the light of our study, the features listed above might be seen with new eyes and reinterpreted as molards, or confirmed as hummocks on collecting new data. Further studies should therefore focus on distinguishing molards from other conical features on landslides in order to avoid confusion in their interpretation.

5. Conclusions

By studying how the deposits of two landslides in northern Iceland evolved through time, we have shown for the first time that molards in permafrost terrains are cones of loose debris that result from the degradation of blocks and ridges of ice-cemented deposits mobilised by landslides. Molards have distinctive spatial and geomorphic characteristics that reveal the dynamics of the landslides that formed them. Isolated molards like those of the Móafellshyrna landslide indicate transport via fall, while densely-grouped elongated molards below the main scarp like those of the Árnesfjall landslide are generated by sliding. We distinguish two different dynamic styles using molards, but future study is required to determine if molard characteristics could reveal other types of landslide motion. The relation between permafrost degradation and slope stability is well documented in the literature (e.g., Beniston et al., 2018; Haeberli et al., 2010; Huggel et al., 2012; Kellerer-Pirklbauer et al., 2012; Phillips et al., 2017), but, in the light of our study, further efforts should be engaged in defining how molards can be used in hazard assessment. The types of landslide from which molards form are likely to become more common as ground temperatures in ice-rich permafrost zones increase, making thaw and slope instabilities in periglacial and glacial environments more probable. Given that the presence of ice enables long runout and high velocity in mass movements (Huggel et al., 2005), molards could be used to signal areas at risk of potentially disastrous ground ice thaw-induced landslides in vulnerable areas. We have demonstrated that molards are a landform that can be readily recognised in the field as a marker of recent and ongoing permafrost degradation. We found relatively few molards in Iceland compared to in previous studies of molards in permafrost-rich terrains, hence the number-density of molards at a site may reveal the abundance of ground ice at the time of the failure. One of our study sites in northern Iceland falls in an area where mountain permafrost was not predicted (Etzelmüller et al., 2007; Rekacewicz, 2005), and until our study there was scarce direct field evidence of permafrost and/or its condition. The recent formation of molards reveals the presence of permafrost in the area, and its ongoing degradation.

Finally, we have demonstrated that molards are not only readily recognisable in the field, but also via remote sensing. This opens up the possibility of efficiently identifying these landforms across large and remote areas, revealing the influence of ice thaw not only in mountain permafrost environments, but also on planetary surfaces such as Mars, where the role of volatiles in landscape evolution is vigorously debated (Conway and Balme, 2016; Dundas et al., 2017; Leverington, 2011).

Author contributions

C.M., S.J.C., Þ.S., J.K.H., and M.R.B. conceived and designed the research. C.M. collected, processed, and analysed the data, and prepared the manuscript. S.J.C. significantly contributed to data collection and analysis and manuscript preparation. Þ.S. and J.K.H. contributed to data collection and manuscript preparation. J.H. contributed to data analysis and manuscript preparation. F.E.G.B. collected data for Mars and contributed to manuscript preparation. M.R.B. and C.J. contributed to data processing and manuscript preparation. T.A. contributed to manuscript preparation.

Competing interests: The authors declare no competing interests.

Acknowledgements

This work has been funded by a postgraduate studentship grant (NE/L002493/1) from the Central England Natural Environment Research Council Training Alliance (CENTA). This project forms part of and is funded by a British Geological Survey BUFI CASE Studentship (GA/14S/024, Ref: 284). We thank the Natural Environment Research Council Airborne Research Facility (NERC ARF) and their Data Analysis Node (NERC-ARF-DAN) plus the EUropean Facility for Airborne Research (EUFAR) for the air photography and LiDAR data on which this paper relies. Thanks go to NERC Geophysical Equipment Facility (GEF) for the Loans 1048 and 1064 through which differential GPS surveys were possible. We thank the GeoPlanet writing residential scheme for the support in writing this manuscript. C. Jordan publishes with permission of the Executive Director of BGS. S. J. Conway is funded by the French Space Agency, CNES, for her HiRISE related work. We gratefully acknowledge the contribution of Gestur Hansson (Icelandic Meteorological Office) and of our field assistants Francesco Giuntoli, Silvia Crosetto, and Sydney Gunnarson. The authors thank the reviewers Anja Dufresne, Marten Geertsema and Gioachino Roberti for their insightful comments.

Appendix A. Supplementary material

Supplementary material related to this article can be found online at https://doi.org/10.1016/j.epsl.2019.03.040.

References

Ashastina, K., Schirrmeister, L., Fuchs, M., Kienast, F., 2017. Palaeoclimate characteristics in interior Siberia of MIS 6-2: first insights from the Batagay permafrost mega-thaw slump in the Yana Highlands. Clim. Past 13, 795–818. https://doi.org/10.5194/cp-13-795-2017.

Beniston, M., Farinotti, D., Stoffel, M., Andreassen, L.M., Coppola, E., Eckert, N., Fantini, A., Giacona, F., Hauck, C., Huss, M., Huwald, H., 2018. The European mountain cryosphere: a review of its current state, trends, and future challenges. Cryosphere 12 (2), 759–794.

Benjamin, J., Rosser, N.J., Dunning, S.A., Hardy, R.J., Kelfoun, K., Szczuciński, W., 2018. Transferability of a calibrated numerical model of rock avalanche run-out: application to 20 rock avalanches on the Nuussuaq Peninsula, West Greenland. Earth Surf. Process. Landf.. https://doi.org/10.1002/esp.4469.

Blais-Stevens, A., Geertsema, M., Schwab, J.W., Van Asch, T.W.J., 2015. Complex landslide triggered in an Eocene volcanic-volcaniclastic succession along Sutherland River, British Columbia, Canada. Environ. Eng. Geosci. 21, 35–45. https://doi.org/10.2113/gseegeosci.21.1.35.

Brideau, M., Stead, D., Hopkinson, C., Demuth, M., Barlow, J., Evans, S., Delaney, K., 2009. Preliminary description and slope stability analyses of the 2008 Little Salmon Lake and 2007 Mt. Steele landslides, Yukon. Yukon Explor. Geol., 119–134.

Brynjólfsson, S., Schomacker, A., Ingólfsson, Ó., 2014. Geomorphology and the Little Ice Age extent of the Drangajökull ice cap, NW Iceland, with focus on its three surge-type outlets. Geomorphology 213, 292–304. https://doi.org/10.1016/j.geomorph.2014.01.019.

Calvari, S., Tanner, L.H., Groppelli, G., 1998. Debris-avalanche deposits of the Milo Lahar sequence and the opening of the Valle del Bove on Etna volcano (Italy). J. Volcanol. Geotherm. Res. 87 (1–4), 193–209.

Carrigy, M.A., 1970. Experiments on the angles of repose of granular materials. Sedimentology 14, 147–158.

Carrivick, J.L., Smith, M.W., Quincey, D.J., 2016. Structure from Motion in the Geosciences. John Wiley & Sons.

Carson, M.A., 1979. Le glissement de Rigaud (Québec) du 3 mai 1978: une interprétation du mode de rupture d'après la morphologie de la cicatrice. Géogr. Phys. Quat. 33, 63. https://doi.org/10.7202/1000323ar.

Cassie, J.W., Van Gassen, W., Cruden, D.M., 1988. Laboratory analogue of the formation of molards, cones of rock-avalanche debris. Geology 16, 735–738. https://doi.org/10.1130/0091-7613(1988)016<0735:LAOTFO>2.3.CO;2.

Charrière, M., Humair, F., Froese, C., Jaboyedoff, M., Pedrazzini, A., Longchamp, C., 2016. From the source area to the deposit: collapse, fragmentation, and propagation of the Frank Slide. GSA Bull. 128, 332–351. https://doi.org/10.1130/B31243.1.

Conway, S.J., Balme, M.R., 2016. A novel topographic parameterization scheme indicates that martian gullies display the signature of liquid water. Earth Planet. Sci. Lett. 454, 36–45. https://doi.org/10.1016/j.epsl.2016.08.031.

Conway, S.J., Balme, M.R., 2014. Decameter thick remnant glacial ice deposits on Mars. Geophys. Res. Lett. 41, 5402–5409. https://doi.org/10.1002/2014GL059980.

Cruden, D.M., 1982. The Brazeau Lake slide, Jasper National Park, Alberta. Can. J. Earth Sci. 19, 975–981. https://doi.org/10.1139/e82-081.

Dahl-Jensen, T., Larsen, L.M., Pedersen, S.A.S., Pedersen, J., Jepsen, H.F., Pedersen, G.K., Nielsen, T., Pedersen, A.K., Von Platen-Hallermund, F., Weng, W., 2004. Landslide and tsunami 21 November 2000 in Paatuut, West Greenland. Nat. Hazards 31, 277–287. https://doi.org/10.1023/B:NHAZ.0000020264.70048.95.

Davies, T., Phillips, C., Warburton, J., 2013. Processes, Transport, Deposition, and Landforms: Flow, Treatise on Geomorphology. Elsevier Ltd.

Dufresne, A., Geertsema, M., Shugar, D.H., Koppes, M., Higman, B., Haeussler, P.J., Stark, C., Venditti, J.G., Bonno, D., Larsen, C., Gulick, S.P.S., McCall, N., Walton, M., Loso, M.G., Willis, M.J., 2018. Sedimentology and geomorphology of a large tsunamigenic landslide, Taan Fiord, Alaska. Sediment. Geol. 364, 302–318. https://doi.org/10.1016/j.sedgeo.2017.10.004.

Dundas, C.M., McEwen, A.S., Diniega, S., Hansen, C.J., Byrne, S., McElwaine, J.N., 2017. The formation of gullies on Mars today. Geol. Soc. (Lond.) Spec. Publ. SP467.5. https://doi.org/10.1144/SP467.5.

Dussage-Peisser, C., Helmstetter, A., Grasso, J., Hantz, D., Desvarreux, P., Jeannin, M., Giraud, A., 2002. Probabilistic approach to rock fall hazard assessment: potential of historical data analysis, 15–26.

Dussauge, C., Grasso, J.-R., Helmstetter, A., 2003. Statistical analysis of rockfall volume distributions: implications for rockfall dynamics. J. Geophys. Res., Solid Earth 108. https://doi.org/10.1029/2001JB000650.

Dyke, A.S., Savelle, J.M., 2000. Major end moraines of Younger Dryas age on Wollaston Peninsula, Victoria Island, Canadian Arctic: implications for paleoclimate and for formation of hummocky moraine. Can. J. Earth Sci. 37, 601–619. https://doi.org/10.1139/e99-118.

Einstein, H.A., 1937. Bedload transport as a probability problem. Sedimentation, 105–108.

Etzelmüller, B., Farbrot, H., Guðmundsson, Á., Humlum, O., Tveito, O.E., Björnsson, H., 2007. The regional distribution of mountain permafrost in Iceland. Permafr. Periglac. Process. 18, 185–199. https://doi.org/10.1002/ppp.583.

Etzelmüller, B., Hoelzle, M., Flo Heggem, E.S., Isaksen, K., Mittaz, C., Mühll, D.V., Ødegård, R.S., Haeberli, W., Sollid, J.L., 2001. Mapping and modelling the occurrence and distribution of mountain permafrost. Nor. Geogr. Tidsskr. – Nor. J. Geogr. 55, 186–194. https://doi.org/10.1080/00291950152746513.

Evans, S.G., Hungr, O., 1993. The assessment of rockfall hazard at the base of talus slopes. Can. Geotech. J.. https://doi.org/10.1139/t93-054.

Farbrot, H., Etzelmüller, B., Guðmundsson, Á., Humlum, O., Kellerer-Pirklbauer, A., Eiken, T., Wangensteen, B., 2007. Rock glaciers and permafrost in Tröllaskagi, northern Iceland. Z. Geomorphol. 51, 1–16. https://doi.org/10.1127/0372-8854/2007/0051S2-0001.

Geertsema, M., Cruden, D.M., Schwab, J.W., 2006a. A large rapid landslide in sensitive glaciomarine sediments at Mink Creek, northwestern British Columbia, Canada. Eng. Geol. 83, 36–63. https://doi.org/10.1016/j.enggeo.2005.06.036.

Geertsema, M., Hungr, O., Schwab, J.W., Evans, S.G., 2006b. A large rockslide – debris avalanche in cohesive soil at Pink Mountain, northeastern British Columbia, Canada. Eng. Geol. 83, 64–75. https://doi.org/10.1016/j.enggeo.2005.06.025.

Glicken, H., 1996. Rockslide-debris Avalanche of May 18, 1980, Mount St. Helens Volcano, Washington.

Glicken, H., Voight, B., Janda, R.J., 1981. Rockslide-debris avalanche of May 18, 1980, Mount St. Helens volcano. In: IAVCEI Symposium on Arc Volcanism. Terra Scientific Publishing Co., Tokyo and Hakone, pp. 109–110.

Goguel, J., Pachoud, A., 1972. Géologie et dynamique de l'écroulement du Mont Granier: dans le Massif de Chartreuse, en novembre 1248. Bull. du Bur. Rech. Geol. Minieres III 1, 29–38.

Gruber, S., Hoelzle, M., 2008. The cooling effect of coarse blocks revisited: a modeling study of a purely conductive mechanism. In: Proc. 9th Int. Conf. Permafr, pp. 557–561.

Haeberli, W., Beniston, M., 1998. Climate change and its impacts on glaciers and pemafrost in the Alps. Ambio 27, 258–265.

Haeberli, W., Noetzli, J., Arenson, L., Delaloye, R., Gärtner-Roer, I., Gruber, S., Isaksen, K., Kneisel, C., Krautblatter, M., Phillips, M., 2010. Mountain permafrost: development and challenges of a young research field. J. Glaciol. 56 (200), 1043–1058.

Hambrey, M.J., Huddart, D., Bennet, M.R., Glasser, N.F., 1997. Genesis of "hummocky moraines" by thrusting in glacier ice: evidence from Svalbard and Britain. J. Geol. Soc. Lond. 154, 623–632. https://doi.org/10.1144/gsjgs.154.4.0623.

Harris, S.A., Pedersen, D.E., 1998. Thermal regimes beneath coarse blocky materials. Permafr. Periglac. Process. 9, 107–120. https://doi.org/10.1002/(SICI)1099-1530(199804/06)9:2<107::AID-PPP277>3.0.CO;2.

Hinzman, L.D., Bettez, N.D., Bolton, W.R., Chapin, F.S., Dyurgerov, M.B., Fastie, C.L., Griffith, B., Hollister, R.D., Hope, A., Huntington, H.P., Jensen, A.M., Jia, G.J., Jorgenson, T., Kane, D.L., Klein, D.R., Kofinas, G., Lynch, A.H., Lloyd, A.H., McGuire, A.D., Nelson, F.E., Oechel, W.C., Osterkamp, T.E., Racine, C.H., Romanovsky, V.E., Stone, R.S., Stow, D.A., Sturm, M., Tweedie, C.E., Vourlitis, G.L., Walker, M.D., Walker, D.A., Webber, P.J., Welker, J.M., Winker, K.S., Yoshikawa, K., 2005. Evidence and implications of recent climate change in Northern Alaska and other Arctic regions. Clim. Change 72, 251–298. https://doi.org/10.1007/s10584-005-5352-2.

Hjort, C., Ingólfsson, Ó., Norðdahl, H., 1985. Late Quaternary geology and glacial history of Hornstrandir, northwest Iceland: a reconnaissance study. Jökull 35, e29.

Höfle, B., Rutzinger, M., 2011. Topographic airborne LiDAR in geomorphology: a technological perspective. Z. Geomorphol., Suppl.bd 55, 1–29. https://doi.org/10.1127/0372-8854/2011/0055S2-0043.

Huggel, C., Zgraggen-Oswald, S., Haeberli, W., Kääb, A., Polkvoj, A., Galushkin, I., Evans, S.G., 2005. The 2002 rock/ice avalanche at Kolka/Karmadon, Russian Caucasus: assessment of extraordinary avalanche formation and mobility, and application of QuickBird satellite imagery. Nat. Hazards Earth Syst. Sci. 5, 173–187. https://doi.org/10.5194/nhess-5-173-2005.

Huggel, C., Clague, J.J., Korup, O., 2012. Is climate change responsible for changing landslide activity in high mountains? Earth Surf. Process. Landf. 37 (1), 77–91.

Hungr, O., Evans, S.G., Bovis, M.J., Hutchinson, J.N., 2001. A review of the classification of landslides of the flow type. Environ. Eng. Geosci. 7, 221–238. https://doi.org/10.2113/gseegeosci.7.3.221.

Iverson, R.M., 1997. The physics of debris flows. Rev. Geophys. 3, 245–296.

Jaboyedoff, M., Oppikofer, T., Abellán, A., Derron, M.H., Loye, A., Metzger, R., Pedrazzini, A., 2012. Use of LIDAR in landslide investigations: a review. Nat. Hazards 61, 5–28. https://doi.org/10.1007/s11069-010-9634-2.

Jermyn, C., Geertsema, M., 2015. An overview of some recent large Landslide 59 Types in Nahanni National Park, Northwest Territories, Canada. Eng. Geol. Soc. Territ. 1, 315–320. https://doi.org/10.1007/978-3-319-09300-0_59.

Jóhannesson, H., 2014. Geological Map of Iceland. Bedrock Geology. Scale: 1:600 000 [WWW Document]. 2nd ed. Náttúrufræðistofnun Íslands – Icelandic Inst. Nat. Hist. http://www.arcgis.com/home/item.html?id=c56c70100e21467891fde8f534da96c3#overview.

Jones, A.P., McEwen, A.S., Tornabene, L.L., Baker, V.R., Melosh, H.J., Berman, D.C., 2011. A geomorphic analysis of Hale crater, Mars: the effects of impact into ice-rich crust. Icarus 211, 259–272. https://doi.org/10.1016/j.icarus.2010.10.014.

Jorge, M.G., Brennand, T.A., 2017. Measuring (subglacial) bedform orientation, length, and longitudinal asymmetry – method assessment. PLoS ONE 12. https://doi.org/10.1371/journal.pone.0174312.

Kellerer-Pirklbauer, A., Lieb, G.K., Avian, M., Carrivick, J., 2012. Climate change and rock fall events in high mountain areas: numerous and extensive rock falls in 2007 at Mittlerer Burgstall, Central Austria. Geogr. Ann., Ser. A 94 (1), 59–78.

Kenner, R., Phillips, M., Hauck, C., Hilbich, C., Mulsow, C., Bühler, Y., Stoffel, A., Buchroithner, M., 2017. New insights on permafrost genesis and conservation in talus slopes based on observations at Flüelapass, Eastern Switzerland. Geomorphology 290, 101–113. https://doi.org/10.1016/j.geomorph.2017.04.011.

Krüger, J., Kjær, K.H., 2000. De-icing progression of ice-cored moraines in a humid, subpolar climate, Kötlujökull, Iceland. Holocene 10, 737–747. https://doi.org/10.1191/09596830094980.

Leverington, D.W., 2011. A volcanic origin for the outflow channels of Mars: key evidence and major implications. Geomorphology 132, 51–75. https://doi.org/10.1016/j.geomorph.2011.05.022.

Lilleøren, K.S., Etzelmüller, B., Gärtner-Roer, I., Kääb, A., Westermann, S., Gumundsson, Á., 2013. The distribution, thermal characteristics and dynamics of Permafrost in Tröllaskagi, Northern Iceland, as Inferred from the Distribution of Rock Glaciers and Ice-Cored Moraines. Permafr. Periglac. Process. 24, 322–335. https://doi.org/10.1002/ppp.1792.

Lyle, R.R., Hutchinson, D.J., Preston, Y., 2004. Landslide processes in discontinuous permafrost, Little Salmon Lake (NTS 105L/1 and 2), south-central Yukon. Yukon Explor. Geol., 193–204.

Matsuoka, N., Hirakawa, K., Watanabe, T., Haeberli, W., Keller, F., 1998. The role of diurnal, annual and millennial freeze-thaw cycles in controlling Alpine slope instability. In: Proc. 7th Int. Conf., vol. 55. Permafrost, Yellowknife, 23–27 June 1998, pp. 711–717.

McConnell, R.G., Brock, R.W., 1903. Report on the great landslide at Frank, Alberta, 1903. Dom. Canada, Dep. Inter. Annu. Rep. VIII, 3–17.

Mercer, J.H., 1963. Glacial Geology of Ohio Range, Central Horlick Mountains, Antarctica.

Milana, J.P., 2016. Molards and their relation to landslides involving permafrost failure. Permafr. Periglac. Process. 27, 271–284. https://doi.org/10.1002/ppp.1878.

Mollard, J., Janes, J., 1984. Airphoto Interpretation and the Canadian Landscape. Energy, Mines, Resour. Canada. 415 p.

Morino, C., 2018. The Hidden Hazard of Melting Ground Ice in Northern Iceland. The Open University.

Paguican, E.M.R., de Vries, B.V.W., Lagmay, A.M.F., 2014. Hummocks: how they form and how they evolve in rockslide-debris avalanches. Landslides 11, 67–80. https://doi.org/10.1007/s10346-012-0368-y.

Pedersen, S.A.S., Larsen, L.M., Dahl-jensen, T., Jepsen, H.F., Krarup, G., Nielsen, T., Pedersen, A.K., von Platen-Hallermund, F., Weng, W., 2002. Tsunami-generating rock fall and landslide on the south coast of Nuussuaq, central West Greenland. Geol. Greenl. Surv. Bull. 191, 73–83.

Pedersen, S.A.S., Dahl-Jensen, T., Jepsen, H., Larsen, L.M., Pedersen, G.K., Nielsen, T., Pedersen, K.A., Weng, W., 2001. Fjeldskred ved Paatuut. Rep. 2001/99. Copenhagen.

Phillips, M., Wolter, A., Lüthi, R., Amann, F., Kenner, R., Bühler, Y., 2017. Rock slope failure in a recently deglaciated permafrost rock wall at Piz Kesch (Eastern Swiss Alps), February 2014. 2017 Earth Surf. Process. Landf. 42 (3), 426–438.

Pohlman, N.A., Severson, B.L., Ottino, J.M., Lueptow, R.M., 2006. Surface roughness effects in granular matter: influence on angle of repose and the absence of segregation. Phys. Rev. E, Stat. Nonlinear Soft Matter Phys. 73. https://doi.org/10.1103/PhysRevE.73.031304.

Rekacewicz, P., 2005. Permafrost distribution in the Arctic [WWW document]. UNEP/GRID-Arendal. http://www.grida.no/resources/7000.

Rödder, T., Kneisel, C., 2012. Influence of snow cover and grain size on the ground thermal regime in the discontinuous permafrost zone, Swiss Alps. Geomorphology 175–176, 176–189. https://doi.org/10.1016/j.geomorph.2012.07.008.

Roering, J.J., Mackey, B.H., Marshall, J.A., Sweeney, K.E., Deligne, N.I., Booth, A.M., Handwerger, A.L., Cerovski-Darriau, C., 2013. "You are HERE": connecting the dots with airborne lidar for geomorphic fieldwork. Geomorphology 200, 172–183. https://doi.org/10.1016/j.geomorph.2013.04.009.

Sæmundsson, Þ., Morino, C., Helgason, J.K., Conway, S.J., Pétursson, H.G., 2018. The triggering factors of the Móafellshyrna debris slide in northern Iceland: intense precipitation, earthquake activity and thawing of mountain permafrost. Sci. Total Environ. 621, 1163–1175. https://doi.org/10.1016/j.scitotenv.2017.10.111.

Schomacker, A., Kjær, K.H., 2008. Quantification of dead-ice melting in ice-cored moraines at the high-Arctic glacier Holmströmbreen, Svalbard. Boreas 37, 211–225. https://doi.org/10.1111/j.1502-3885.2007.00014.x.

Schwab, J.W., Geertsema, M., Evans, S.G., 2003. Catastrophic rock avalanches, west-central BC, Canada. In: 3rd Canadian Conference on Geotechnique and Natural Hazards. Edmonton, AB, pp. 52–259.

Séjourné, A., Costard, F., Fedorov, A., Gargani, J., Skorve, J., Massé, M., Mège, D., 2015. Evolution of the banks of thermokarst lakes in Central Yakutia (Central Siberia) due to retrogressive thaw slump activity controlled by insolation. Geomorphology 241, 31–40. https://doi.org/10.1016/j.geomorph.2015.03.033.

Shea, T., van Wyk de Vries, B., 2008. Structural analysis and analogue modeling of the kinematics and dynamics of rockslide avalanches. Geosphere 4, 657. https://doi.org/10.1130/GES00131.1.

Shea, T., van Wyk de Vries, B., Pilato, M., 2008. Emplacement mechanisms of contrasting debris avalanches at Volcán Mombacho (Nicaragua), provided by structural and facies analysis. Bull. Volcanol. 70, 899–921. https://doi.org/10.1007/s00445-007-0177-7.

Shreve, R.L., 1968. The Blackhawk Landslide, vol. 108. Geological Society of America.

Siebert, L.E.E., 1984. Large volcanic debris avalanches: characteristics of source areas, deposits and associated eruptions. J. Volcanol. Geotherm. Res. 22, 163–197.

Smith, M.W., Carrivick, J.L., Quincey, D.J., 2015. Structure from motion photogrammetry in physical geography. Prog. Phys. Geogr. 40, 247–275. https://doi.org/10.1177/0309133315615805.

Ui, T., 1983. Volcanic dry avalanche deposits—identification and comparison with nonvolcanic debris stream deposits. J. Volcanol. Geotherm. Res. 18, 135–150.

Ui, T., Kawachi, S., Neall, V.E., 1986. Fragmentation of debris avalanche material during flowage—Evidence from the Pungarehu Formation, Mount Egmont, New Zealand. J. Volcanol. Geotherm. Res. 27 (3–4), 255–264.

Van Burkalow, A., 1945. Angle of repose and angle of sliding friction: an experimental study. Geol. Soc. Am. Bull. 56, 669–707.

Van Tatenhove, F.G.M., Olesen, O.B., 1994. Ground temperature and related permafrost characteristics in west Greenland. Permafr. Periglac. Process. 5, 199–215.

Varnes, D.J., 1978. Slope Movement Types and Processes. Transp. Res. Board Spec. Rep. 11–33. Special report 176: Landslides: Analysis and Control, Transportation Research Board, Washington, D.C. https://doi.org/In.

Voight, B., Glicken, H., Janda, R.J., Douglass, P.M., 1981. Catastrophic rockslide avalanche of May 18. In: Lipman, P.W., Mullineaux, D.R. (Eds.), The 1980 Eruptions of Mount St. Helens, Washington: U.S.. In: Geological Survey Professional Paper, vol. 1250, pp. 347–377.

Westoby, M.J., Brasington, J., Glasser, N.F., Hambrey, M.J., Reynolds, J.M., 2012. "Structure-from-motion" photogrammetry: a low-cost, effective tool for geoscience applications. Geomorphology 179, 300–314. https://doi.org/10.1016/j.geomorph.2012.08.021.

Xu, Q., Shang, Y., van Asch, T., Wang, S., Zhang, Z., Dong, X., 2012. Observations from the large, rapid Yigong rock slide – debris avalanche, southeast Tibet. Can. Geotech. J. 49, 589–606. https://doi.org/10.1139/t2012-021.

Yarnold, J.C., Lombard, J.P., 1989. A facies model for large rock-avalanche deposits formed in dry climates. In: Abbott, P., Colburn, I.E. (Eds.), Conglomerates in Basin Analysis: A Symposium Dedicated to A.O. Woodford: Society of Economic Paleontologists and Mineralogists Pacific Section, vol. 62, pp. 9–31.

Yoshida, H., Sugai, T., Ohmori, H., 2012. Size-distance relationships for hummocks on volcanic rockslide-debris avalanche deposits in Japan. Geomorphology 136, 76–87. https://doi.org/10.1016/j.geomorph.2011.04.044.

Yoshikawa, K., Hinzman, L.D., 2003. Shrinking thermokarst ponds and groundwater dynamics in discontinuous permafrost near Council, Alaska. Permafr. Periglac. Process. 14, 151–160. https://doi.org/10.1002/ppp.451.